Fuel 316 (2022) 123310

Contents lists available at ScienceDirect

Fuel

journal homepage: www.elsevier.com/locate/fuel

Full Length Article

Real coupling of solid oxide fuel cells with a biomass steam gasifier: Operating boundaries considering performance, tar and carbon deposition analyses

Gernot Pongratz [a,*], Vanja Subotić [a], Lukas von Berg [a], Hartmuth Schroettner [b], Christoph Hochenauer [a,c], Stefan Martini [c], Maximilian Hauck [d], Benjamin Steinruecken [d], Marek Skrzypkiewicz [e,f], Jakub Kupecki [e,f], Robert Scharler [a,c], Andrés Anca-Couce [a]

[a] Institute of Thermal Engineering, Graz University of Technology, Inffeldgasse 25b, 8010 Graz, Austria
[b] Institute for Electron Microscopy and Nanoanalysis, Graz University of Technology, Steyrergasse 17, 8010 Graz, Austria
[c] BEST – Bioenergy and Sustainable Technologies GmbH, Inffeldgasse 21b, 8010 Graz, Austria
[d] Chair of Energy Systems, Technical University of Munich, Boltzmannstrasse 15, 85747 Garching, Germany
[e] Center for Hydrogen Technologies (CTH_2), Institute of Power Engineering, Augustówka 36, 02-981 Warsaw, Poland
[f] Institute of Power Engineering, Mory 8, 01-330 Warsaw, Poland

ARTICLE INFO

Keywords:
Solid oxide fuel cell
Biomass gasification
Tar content
Carbon deposition
Degradation effects

ABSTRACT

Solid oxide fuel cells are a promising alternative to gas engines for combined heat and power production based on biomass gasification. The technical complexity of realizing gasifier – fuel cell couplings has limited the number of experiments conducted in the past. However, results from such experiments are of high importance for the evaluation of tar thresholds and operating conditions ensuring a stable operation of fuel cells. For the first time, it was possible to demonstrate for dozens of hours the operation of solid oxide fuel cells with real product gas from steam gasification with a steam-to-carbon ratio of 2 and a typical tar content for fluidized bed gasification. Four coupling experiments with industrial-relevant cell designs were conducted, demonstrating a stable operation for 30 h without structural degradation of the anodes for cells with nickel/ceria- and nickel/zirconia-based anodes at 800°C and 850°C, if heavy tars were partially removed (2.8–3.7 g·Nm^{-3} gravimetric tars). Raw gas operation (4.6–4.8 g·Nm^{-3} gravimetric tars) led to metal dusting effects on nickel contact meshes and nickel/zirconia-based anodes, whereas nickel/ceria-based anodes were less affected. Carbon deposited on the alumina support in all experiments whereby a change from pyrolytic to graphitic structure could be observed when increasing the temperature from 800°C to 850°C, thus significantly reducing the risk for blockages in the flow channels. Moreover, high tar and benzene conversion rates were observed. Concluding, operating temperatures of 850°C and the removal only of heavy tars can enable stable long-term operation with a tar-laden steam gasifier product gas, even without increasing the steam-to-carbon ratio to values exceeding two.

1. Introduction

The world's demand for sustainable energy is steadily increasing. To keep global warming below 1.5 °C, the Intergovernmental Panel on Climate Change recently underlined the urgency to reach zero net-CO_2 emissions around 2050 [1]. Generating power from solid biomass is a promising carbon–neutral technology to achieve this ambitious goal. However, the electrical efficiency of biomass gasification-based combined heat and power (CHP) systems using gas engines as power generators is limited to 25–30%. By using solid oxide fuel cell (SOFC) stacks instead of gas engines, the potential is given for increasing the electrical efficiency to values exceeding 40% [2,3]. Since fuel consumption and therefore costs are crucial for power generation from biomass, an increase in electrical efficiency is essential to make this technology more economically attractive [4]. A number of challenges must be solved in order to ensure stable SOFC operation with minimal performance degradation over an industrial-relevant lifetime and consequently to introduce biomass gasification-based CHP systems using SOFCs on the market. Besides still high capital expenditures (CAPEX) of SOFC systems, also gas cleaning upstream of SOFC stacks must be more intensive compared to gas engines which increases the CAPEX for the overall CHP

* Corresponding author.
E-mail address: gernot.pongratz@tugraz.at (G. Pongratz).

https://doi.org/10.1016/j.fuel.2022.123310
Received 7 August 2021; Received in revised form 14 January 2022; Accepted 16 January 2022
Available online 25 January 2022

Nomenclature

Abbreviations

ASC	anode supported cell
CAPEX	capital expenditures
CHP	combined heat and power
d.b.	dry basis
EDX	energy-dispersive X-ray spectroscope
EIS	electrochemical impedance spectroscopy
ESC	electrolyte supported cell
FBS	fluidized bed steam
FDA	fixed bed downdraft air
GC	gas chromatography
MS	mass spectrometry
Ni/GDC	nickel/gadolinium-doped ceria
Ni/YSZ	nickel/yttria-stabilized zirconia
SCR	steam-to-carbon ratio
SEM	scanning electron microscope
slpm	standard liter per minute
SOFC	solid oxide fuel cell
w.b.	wet basis

List of symbols

A	active cell surface in cm^2
F	Faraday's Constant in $As \cdot mol^{-1}$
i	cell current density in $mA \cdot cm^{-2}$
LHV	lower heating value in $MJ \cdot Nm^{-3}$
n_{el}	number of electrons
n_{FuelIn}	molar flux of fuel at inlet in $mol \cdot s^{-1}$
n_i	molar flux of gas component i in $mol \cdot s^{-1}$
OCV	open circuit voltage in V
P	power output of cell
R_Ω	ohmic resistance in $\Omega \cdot cm^2$
R_{Pol}	polarization resistance in $\Omega \cdot cm^2$
U	cell voltage in V
U_f	fuel utilization in %
V_A	anodic volume flow in slpm
V_C	cathodic volume flow in slpm

system. Lowering the gas purification level would significantly decrease these costs thus making SOFCs a competitive alternative to gas engines.

High-temperature gas cleaning methods are recommended for CHP systems using SOFCs as power generators to achieve high system efficiencies, which can be attributed to the lower amount of energy required to preheat the fuel gas to SOFC operating temperatures after the purification steps [5]. Ceramic filter candles offer high cleaning efficiencies for particulate matter at temperatures near to gasifier operation, whereby inorganic impurities as H_2S and HCl can be reduced to sub-ppm_v levels in fixed bed reactors filled with high-temperature sorbents based on metal-oxides and alkaline earth metal compounds, respectively [6]. The reduction of tars (organic molecules with molecular weights greater than benzene according to [42]) appears to be more complex and error-prone than H_2S, HCl or particulate separation and can be realized at high temperatures via several non-catalytic (e.g. partial oxidation, which reduces the efficiency and generates soot) or catalytic (steam/dry reforming over nickel, which is prone to deactivation) methods [6,7]. The thresholds for particulate matter, H_2S and HCl, organic sulfur compounds and tars in biomass gasification product gas for the use in SOFCs still give cause for discussion. While there is general consensus on the need to keep H_2S, HCl, and particulate matter levels as low as possible or at least in the range of a few ppm_v, recommendations for acceptable tar levels range from tens to several hundred ppm_v [6,8–12]. Hence, exploring the limits for acceptable tar contents in product gas from biomass gasification might hold the largest potential for the reduction of gas cleaning requirements and consequently total costs.

The varying recommendations for the acceptable tar level can be attributed to the different effect of tar components on nickel-based catalysts like SOFC anodes. On the one hand, tars can decompose to some extent on nickel catalysts providing extra H_2 and CO as fuel for electrochemical reactions, thus increasing the cell performance. Higher temperatures and steam-to-carbon ratios (SCR) favor the decomposition of tars, whereas the reactivity of following five model compounds was demonstrated in [13] as follows: benzene > toluene > anthracene > pyrene > naphthalene. On the other hand, tar molecules like benzene or naphthalene are claimed as catalyst poisons for anodic nickel in [14] and [15] thus hindering methane reforming reactions and the electrochemical oxidation of H_2 and CO. Moreover, phenol might lead to dusting of anodic nickel as demonstrated in [16]. With regard to the anode material, anodes based on nickel/gadolinium-doped ceria (Ni/GDC) are less prone to carbon deposition and catalyst poisoning due to tar decomposition than anodes based on nickel/yttria-stabilized zirconia (Ni/YSZ), predominantly due to the mixed ion- and electrical conductivity as well as catalytic properties of ceria [8,17]. In summary, tar thresholds strongly depend on (i) the cell operating temperature, (ii) the main fuel gas composition and the type of tars in the gas mixture as well as on (iii) the SOFC anode material and design.

The gasifier design acts as a main precursor for tar formation. Table 1 gives an overview of state-of-the-art gasifier designs and their characteristics based on [18] and [19]. The technical complexity of realizing gasifier - SOFC coupling has limited the number of experiments conducted in the past. Table 2 summarizes experimental efforts that have so far been made in demonstrating SOFC operation with product gas from biomass gasification together with their outcomes in terms of performance stability, carbon deposition and structural cell degradation. Whereas a tar conditioning unit is crucial for updraft gasifier designs when coupling to fuel cells, tar contents in the product gas of fixed-bed downdraft gasifiers might already be low enough for stable SOFC operation as released gaseous compounds pass a hot oxidation zone in which heavy tars are cracked [20]. However, in addition to the disadvantage of a lower possible power range and fuel flexibility, fixed bed gasifiers are predominantly operated with air as the gasification agent resulting in an SCR usually below 1 together with a low H_2/CO yield. A low SCR significantly increases the risk for carbon deposition according to [21–26], whereby a low H_2/CO ratio has a negative effect on the performance of an SOFC [27]. The addition of steam or oxygen to the air to increase the H_2O concentration in the product gas and to consequently reduce the carbon deposition risk is only possible to a certain extent due to various technological limitations [20]. In the past, stable gasifier – SOFC couplings for more than 100 h could only be demonstrated using air gasifiers with product gas showing almost no tar content [28–30] (details see Table 2). However, SCRs below 1 resulted in carbon deposition, especially at SOFC operating temperatures below 850°C [5,30].

In contrast, fluidized bed gasifier designs offer the opportunity of working exclusively with steam as the gasification agent when using an

Table 1
Gasifier designs and typical characteristics [18].

Gasifier design	Power range [MW_{th}]	Tar content [$g \cdot Nm^{-3}$]	Fuel flexibility
Fixed bed downdraft	< 2	< 1	low
Fixed bed downdraft staged	< 10	< 0.1	medium
Fixed bed updraft	< 5	< 100	high
Fluidized bed	< 50	< 10	high

Table 2
Overview of operating conditions and outcomes of coupling experiments conducted in the past in chronological order with SCRs according to Eq. (1) and U_f as the fuel utilization according to Eq. (2). ASC and ESC represent anode and cathode supported cells, respectively.

Ref.	Gasifier design	SCR	Tar content	Cell type and temperature	U_f	Coupling duration	Conclusion
[29]	Staged fixed bed downdraft	0.9	< 1 mg·Nm^{-3}	Ni/GDC ESC at 850°C	30%	150 h	Negligible performance degradation after 150 h of coupling single cell to gasifier. Authors suggested focus on tests with higher tar contents in the future.
[33]	Fixed bed downdraft	7–10.4	< 1 g·Nm^{-3}	Ni/GDC ESC at 850°C	33%	44 h	No performance loss observed. High SCR due to steam injection. Followed by coupling to fluidized bed gasifier before disassembly (see next line).
[33]	Fluidized bed	5.9–6.7	3 g·Nm^{-3}	Ni/GDC ESC at 850°C	33%	7 h	No performance loss and carbon deposits for single cell after 7 h of operation at 3 g·Nm^{-3} tars.
[32]	Fluidized bed	7	10 g·Nm^{-3}	Ni/GDC ESC at 850°C	22%	8 h	No performance degradation during 8 h of coupling single cell to gasifier. No structural degradation of the anode or carbon deposits reported.
[28]	Staged downdraft	1.5	< 1 mg·Nm^{-3}	Ni/YSZ ASC at 700°C	90%	145 h	No performance degradation of 50-cell stack observed during 145 h of coupling if no tar is present in the feed gas.
[16]	Fluidized bed	7	0–5 g·Nm^{-3}	Ni/YSZ ASC at 715°C	40%	15 h (no tars) 8 h (5 g·Nm^{-3} tars)	No performance degradation of 4-cell stack after 15 h operation on tar-free gas. When bypassing tar reformer, significant increase of pressure loss over stack and performance reduction observed after 8 h. Posttest analyses revealed metal dusting of anode and carbon deposits blocking flow channels.
[30]	Staged fixed bed downdraft	0.33	< 1 g·Nm^{-3}	Ni/YSZ ASC at 680°C	8%	120 h	Carbon deposition for 5-cell stack coupled with biomass gasifier investigated at low SCR. Stack performance decreased comparably to previous single cell experiments. As expected, severe carbon deposition in the inlet region of all 5 cells observed.

additional combustion reactor to provide heat for the endothermic steam gasification reactions in a dual fluidized bed configuration [31]. This leads to significantly higher SCRs and H_2/CO ratios in the product gas thus reducing the thermodynamic risk for carbon formation and increasing the cell performance, respectively [27]. Moreover, the high fuel flexibility and scalability makes this gasifier design very attractive for the use with SOFCs. The higher tar content in the product gas, however, might be the major drawback for the direct use of product gas from steam gasification as discussed in [5]. In the past, successful operation of SOFCs with real steam gasifier product gas in terms of a stable cell performance and undamaged anode was relying on a SCR greater than 6 besides a complete tar removal at operating temperatures below 850°C [16,32,33]. Moreover, experiments using product gas with a non-negligible amount of tars were limited to a maximum of 8 h. These operating conditions, however, may not reflect the requirements of an industrial application. A high SCR significantly reduces the lower heating value (LHV) of the product gas and consequently the expectable electrical efficiency and power output of the fuel cells [54]. Furthermore, the need for a complete removal of tars from the product gas would be a very challenging task, especially when also considering possible deactivation of catalytic tar reforming units, hindering the development of this technology [6,7]. For this reason, results from operating SOFCs with real product gas from steam gasification showing lower SCRs and the presence of tars are of high value due to a potential in reducing gas cleaning requirements besides increasing the cell performance.

For the first time, it was possible to demonstrate the operation of solid oxide fuel cells with real product gas from steam gasification with a more industrial-relevant SCR of 2 and a typical amount of tars for fluidized bed gasification for dozens of hours. This work provides results of four coupling experiments lasting from 30 to 60 h with analyses of i) changes in cell performance and resistances, ii) irreversible structural degradation of the anode and contacting meshes, iii) carbon deposits on the cells and their housing as well as iv) tar reforming capabilities of the cells. The test conditions were iteratively developed throughout the experimental campaign in order to generate a broad range of insights into the behavior and stability of industrial-relevant cell types at temperatures and tar concentrations interesting for the scientific community. A direct comparison of the used cell types was not the objective of this paper, especially when considering the slightly varying operating conditions in each experiment. Concluding, the obtained results might be of high value for the further evaluation of required operating conditions for a stable coupling of SOFCs with fuel-flexible fluidized bed steam gasifiers - a promising configuration for targeting a high electrical system efficiency.

2. Experimental setup and applied methods

2.1. Setup and equipment

The coupling test bench consisted of a lab-scale fluidized bed steam (FBS) gasifier, a gas conditioning unit and a SOFC test bench, as schematically shown in Fig. 1. The cells could be fueled either with H_2/H_2O/N_2 gas mixtures or the product gas of the FBS gasifier. Fuel cells were placed in a non-sealed alumina housing with nickel and platinum meshes used for electrical contacting of the anode and cathode side, respectively. Detailed information about the cell assembly can be found elsewhere [34–36]. Reduction of the cell anodes with increasing H_2 contents (in N_2) was conducted in accordance to the guidelines of the cell suppliers. Subsequently, the quality of the cell assemblies was validated by recording polarization curves and impedance spectra and comparing them with previous experiments. Coupling experiments were performed only with cell assemblies showing a good electrical contact, low leakage and consequently a reasonable power range.

The gasification reactor was operated at 750°C and 2 bar absolute pressure in all coupling experiments. Wood pellets (composition see [37]) with a LHV of 17.6 MJ·kg^{-1} and approximately 10 vol% moisture content were fed to the bubbling fluidized bed reactor at a rate of 298 g·h^{-1}, corresponding to a fuel input power of 1.5 kW. They were gasified with steam at a steam-fuel equivalence ratio of 4, which resulted in approximately 12 standard liters per minutes (slpm) of wet product gas leaving the gasifier. The averaged gas composition, LHV and SCR of the product gas over the whole experimental campaign are shown in Table 3. The LHV was calculated considering H_2, CO and CH_4 neglecting other hydrocarbons present in the product gas. The water content of the raw- and conditioned product gas was determined via a gravimetric

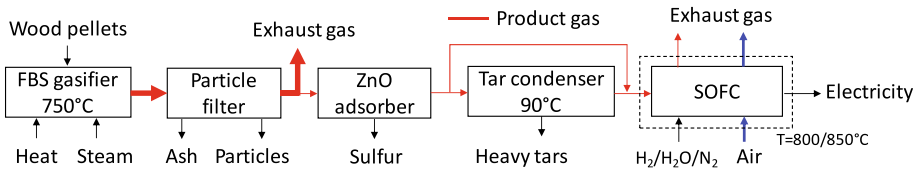

Fig. 1. Scheme of the coupling test bench.

Table 3
Average product gas composition on a dry basis (d.b.) over the whole measurement campaign, N_2 balanced. LHV considering H_2, CO and CH_4, SCR according to Eq. (1), standard deviations in brackets.

H_2	vol% d.b.	36.4 (1.8)
CO	vol% d.b.	14.7 (1.3)
CO_2	vol% d.b.	17.4 (0.7)
CH_4	vol% d.b.	6.4 (0.2)
N_2	vol% d.b.	24.6 (2.9)
LHV	$MJ \cdot Nm^{-3}$ d.b.	8.2 (0.4)
SCR	–	2 (0.2)

method. The SCR was calculated according to Eq. (1), neglecting larger hydrocarbons with $\dot{n}_i$ as the molar fluxes of the gas components.

$$SCR = \frac{\dot{n}_{H_2O}}{\dot{n}_{CO} + \dot{n}_{CH4}} \quad (1)$$

After the particle filter, a partial stream of the product gas was directed to the SOFC test bench. Details of the gasifier can be found in [38] and [39]. Additional gas cleaning was conducted before the SOFC test bench in order to enhance the lifetime of the cells. In a ZnO-based desulfurization reactor, H_2S and COS contents were reduced below the detection limit of a gas chromatograph with sulfur-sensitive pulsed flame photometric detector. The product gas contained less than 1 ppm_v HCl, which was negligible for the operation according to [40]. Moreover, a tubular heat exchanger operated at 90°C was used to condense heavy tars while maintaining the water content of the product gas. Tar condensation rates were evaluated via tar measurements and a condensation model presented in [41]. This tar condenser could be bypassed to feed desulfurized raw product gas to the cell. Subsequently, desulfurized gas directed through the tar condenser will be given the descriptive addition "conditioned", or "raw" when the condenser was bypassed. All pipes, the particle filter and the desulfurization unit were heated to 350°C to minimize tar condensation. More details of the test rig can be found in the supplementary material (Fig. S1). In real biomass gasification-based CHP systems, product gas cleaning is favored at temperatures close to SOFC operation in order to keep the overall system efficiency high [5]. As discussed in the introduction section, hot gas tar reduction can be realized via catalytic or non-catalytic techniques, whereby the operating temperature of desulfurization units based on metal-oxide sorbents can be increased by using Cu- or Ce-based oxides as comprehensively reviewed in [6].

Tars were collected directly before and after the SOFC oven following the international standard DIN CEN/TS 15,439 known as "tar protocol" by quenching the product gas in cooled impingers filled with isopropanol, as schematically shown in [37]. In general, tars can be defined as organic molecules with molecular weights greater than benzene according to [42] and can be classified as shown in Table 4. It is possible to collect nearly 100% of tars and most of benzene in the impingers using the tar protocol setup [43]. Additionally, the water content of the product gas was determined by weighing the impingers before and after the tar protocol. The content of gravimetric tars was determined by separating isopropanol and water from the impinger liquid using a rotary evaporator. Benzene, most of class 3 tars and even a fraction of class 4 and 2 tars are however not captured in the gravimetric residue due to the low boiling point of these components. Therefore, cooled liquid samples from the tar protocol were subsequently analyzed

Table 4
Classification of tars according to [42]

Class	Description
1	Undetectable by gas chromatography
2	(e.g. biomass fragments) Heterocyclic compounds
3	(e.g. phenol, cresol) 1 ring aromatics
4	(e.g. toluene, xylenes) Light polyaromatic hydrocarbons (2–3 rings) (e.g. naphthalene, indene)
5	Heavy polyaromatic hydrocarbons (≥4 rings) (e.g. pyrene, fluoranthene)

using gas chromatography (GC) coupled to mass spectrometry (MS) to determine the content of benzene and toluene (as representative of light condensable tars).

For the online analysis of the product gas, a permanent gas analyzer (ABB AO2020) was used measuring the H_2, CO, CO_2 and CH_4 content. The volume flow of the product gas entering the SOFC setup was determined by measuring the differential pressure over an orifice and calculating the flow considering the gas composition and orifice temperature. Fluctuations of the gas pressure in the sampling pipes resulted in fluctuations of the volumetric flow through the cell. Due to the relatively low fuel utilizations, these fluctuations had a negligible impact on the cell voltage which was also observed in [33]. Electrical characterization of the cells by the means of polarization curves and electrochemical impedance spectroscopy (EIS) was conducted using a Bio-Logic analyzer in combination with an 80 A / 3 V booster. Details about the measurement parameters can be found elsewhere [34]. The temperature distribution within the anodic compartments was determined using three type K thermocouples. Post-mortem analyses of the microstructure were conducted using a Zeiss Ultra 55 platform equipped with a field emission scanning electron microscope (SEM) and an energy-dispersive X-ray spectroscope (EDX).

2.2. Test conditions

Four coupling experiments were conducted with industrial-relevant cells with physical dimensions of 100 mm × 100 mm and 80 cm^2 of active cell surface. The test conditions are summarized in Table 5 with V_A and V_C as the anodic and cathodic volume flow in standard liter per minute (slpm), respectively, LHV as the lower heating value and U_f as the fuel utilization factor. U_f was calculated according to Eq. (2) as proposed in [44] with i as the current density, F as the Faraday's Constant, A as the active cell surface, $\dot{n}_{FuelIn}$ as the molar flow of the fuel components H_2, CO and CH_4 and n_{el} as the sum of electrons involved in the oxidation reactions of these components. In tests A and B, 30 h of coupling with conditioned product gas (tar condenser used) was followed by a coupling period using raw product gas (tar condenser bypassed, descriptive addition "Raw"). At low fuel utilizations as presented in Table 5, the risk for carbon deposition is higher than at industrial-relevant high fuel utilizations as the average H_2O concentration in the flow field and consequently the local SCRs do not significantly change in comparison to the composition at the cell inlet [23].

Table 5
Test conditions for the coupling experiments (d.b.: dry basis, w.b.: wet basis, standard deviations in bracket). In tests A and B, 30 h of coupling with conditioned product gas (tar condenser used) was followed by a coupling period using raw product gas (tar condenser bypassed).

Test ID:	A	A Raw	B	B Raw	C	D
Cell ID	I		II		III	IV
Design	ESC		ESC		ASC	ASC
Anode	Ni/GDC		Ni/YSZ		Ni/YSZ	Ni/YSZ
Cell details	[45]		[46]		[47]	[48]
Temperature in °C	850		850		800	850
Electrical load in mA·cm^{-2}	200		100		100	100
Duration in h	30	30	30	12	30	30
V_A in slpm w.b.	1.34 (0.05)	1.49 (0.06)	1.08 (0.1)	1.1 (0.09)	1.04 (0.12)	1.2 (0.19)
V_C in slpm	2					
Gas composition	see Table 3					
U_f in %	15.9	13.5	9.1	8.9	9.4	8.3
Tar condensation at 90°C	yes	no	yes	no	yes	yes
Gravimetric tars content in g·Nm^{-3} d.b.	3.7	4.8	2.8	4.6	3.2	3.4

Thus, cell operation was conducted at low fuel utilizations in order to accelerate carbon deposition. Higher fuel utilizations are targeted in industrial applications in order to increase the electrical efficiency of fuel cell systems and to reduce the number of cells required to generate a certain power output.

$$U_f = \frac{I}{Fn_{el}\dot{n}_{FuelIn}} = \frac{iA}{F(2\dot{n}_{H2} + 2\dot{n}_{CO} + 8\dot{n}_{CH4})} \quad (2)$$

Four cells with 3 different cell designs were used in the experimental study: an electrolyte supported cell (ESC) with Ni/GDC-based anode (cell I), an ESC with Ni/YSZ-based anode (cell II) and two anode supported cells (ASC) with Ni/YSZ-based anode (cell III, cell IV). Details of the cells can be found in the references listed in Table 5. As discussed in the introduction section, no comparable coupling experiments have been conducted in the past. Therefore, the investigated test conditions presented in Table 5 were iteratively developed throughout the experimental campaign. A direct comparison of the used cell types was not the objective of this paper, especially when considering the slightly varying operating conditions in each experiment. For test A, a Ni/GDC ESC (cell I) and operating temperature of 850°C were chosen as Hofmann et al. demonstrated a successful coupling for 7 h using gasifier product gas with an SCR of 7 containing more than 10 g·Nm^{-3} tars [32]. The results of each experiment worked as basis for the definition of cell-type and operating conditions for the subsequent experiment. Product gas composition, flow rate and tar content slightly varied due to unavoidable small changes in fluidization conditions, feeding rate and biomass composition after each shut-down and start-up of the lab-scale gasifier, whereby negligible low fluctuations were observed during the coupling experiments.

2.3. Test procedure

The test procedure is schematically shown in Fig. 2. Before each coupling experiment, a dry reference gas mixture containing 50 vol% H_2 in N_2 was fed to the cell to provide a common frame of reference for EIS analyses and polarization curve comparisons (blue lines). Moreover, a tar protocol and permanent gas analysis were conducted before each coupling experiment to determine the tar composition and permanent gas distribution of the feed gas. After coupling the cells to the gasifier (red lines), a steady open circuit voltage (OCV), anodic volume flow and temperature distribution within the cell holder was first awaited for determining the chemical activity and electrochemical potential of the cells. The electrical load was then applied and a tar protocol at the cell outlet was started, lasting for approx. 5 h. EIS measurements were conducted every 30 min, whereas fast polarization curves were recorded every hour by removing the electrical load at a rate of 1 A·s^{-1} followed by an immediate loading at the same rate. The reference gas mixture (50/50 vol% H_2/N_2) was applied after each coupling experiment and EIS measurements as well as a fast polarization curve were recorded after a stabilization period of 30 min and again after 10 h. This was intended to clarify whether possible performance degradation could be recovered. A standby gas mixture (green lines) of 10 vol% H_2 in N_2 was applied between these reference measurements. At first, 30 h of cell operation on conditioned product gas was conducted to reduce the quantity of heavy tars reaching the cell. If no significant performance degradation could be observed, raw product gas was subsequently applied for 30 h (tests A and B). After completion of the experiment, a post-mortem investigation was conducted during which the alumina cell holder as well as the anodic feed- and off-gas pipes were examined for carbon deposits. Structural changes of the anode and nickel contact meshes were

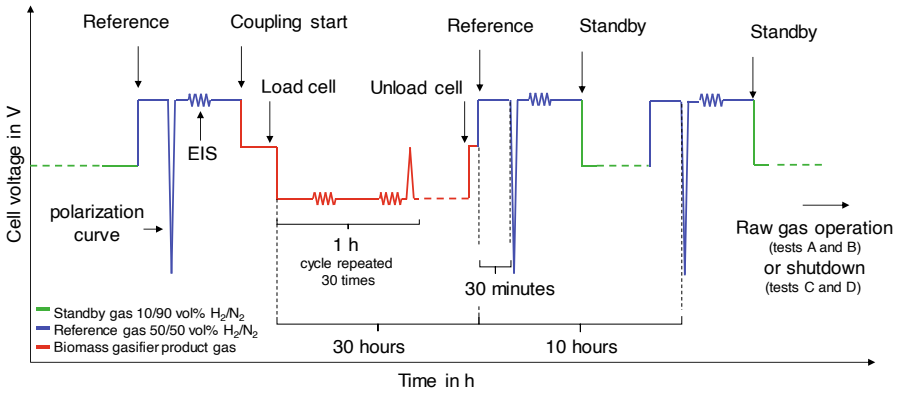

Fig. 2. Schematic representation of the test procedure. Colored lines indicate different feed gas compositions.

analyzed via microscopic methods (SEM and EDX). After each test, the alumina cell support and pipes were heated to 800°C for 5 h in air atmosphere in order to remove any carbon deposits via oxidation.

3. Results and discussion

This section presents the results of performance, tar and post-mortem analyses of the coupling experiments A-D.

3.1. Performance analyses

On the one hand, performance analyses were conducted by the means of comparing changes in the OCV and power output *P* at the current densities presented in Table 5 during coupling with the FBS gasifier (see Fig. 3). Open circuit voltages were considered from the fast polarization curves recorded every hour. Moreover, the evolution of changes in ohmic- and polarization resistances of the cells, R_Ω and R_{Pol}, were analyzed. On the other hand, changes in OCV, power output at 0.7 V and cell resistances at reference conditions (50/50 vol% H_2/N_2) were compared as shown in Fig. 4 and the results used to discuss possible sources for degradation observed during coupling. Details about the changes in gas composition due to open and closed circuit operation of the SOFCs can be found in the supplementary material in Fig. S2. Due to the varying test conditions presented in Table 5, the consideration of voltage and resistance changes instead of absolute values were employed to avoid conflicts of interest between the cell suppliers.

3.1.1. Test A - Ni/GDC ESC 850°C

In test A, a Ni/GDC ESC (cell I) was operated with conditioned (heavy tars were removed by condensation) and raw product gas for 30 h each at an operating temperature of 850°C. The cell did not show significant changes in cell performance and OCV during 30 h of operation with conditioned product gas and subsequent 30 h of operation with raw product gas as shown in Fig. 3a. The gas composition at the cell outlet stayed unchanged during the coupling procedure. R_{Pol} remained constant during operation, whereas a slight increase of R_Ω with a following steady state could be observed as depicted in Fig. 3b. The higher fluctuation of R_{Pol} in comparison to R_Ω might be attributed to the larger impact of flow fluctuations on the impedance measurements at low frequencies, which could also be observed during tests B-D. Fig. 4b shows a performance loss of approx. 3% 30 min after coupling (measured at reference conditions), which could be almost completely recovered after 10 h under standby conditions. This indicates the absence of irreversible performance degradation. When employing raw product gas containing heavy tars, however, an irreversible performance loss of 3% could be observed after 30 h of coupling. Taking Fig. 4b into consideration, this loss might be attributed to the irreversible increase of R_Ω of approx. 5% whereas R_{Pol} could be almost completely recovered (approx. 2% left). According to post-mortem analyses (discussed in section 3.3.1 in more detail), this irreversible increase of R_Ω might be attributed to beginning metal dusting effects on the nickel contact mesh and consequently a decrease of electrical contact between the mesh and the anode. Thus, nickel dusting effects on the cell anode might not be excluded for long-term operation.

3.1.2. Test B - Ni/YSZ ESC 850°C

Cells with Ni/YSZ-based anode are claimed to be more sensitive to tar components in the fuel gas than cells with Ni/GDC-based anode as stated in [17] and [8]. The procedure applied for cell I was later repeated for cell II (Ni/YSZ ESC) in test B, in order to quantify the mentioned higher sensitivity under the operating conditions specified in Table 5. Moreover, a lower electrical load was applied to increase the probability for carbon deposition according to [49]. During the operation with conditioned product gas, a slight performance decrease at unchanged OCV (see Fig. 3c) and outlet gas composition (see supplementary material Fig. S2d) could be observed. This is connected to increasing cell resistances as shown in Fig. 3d. Measurements during operation with the reference gas indicated a significant performance loss of approx. 11% 30 min after the end of the coupling (see Fig. 4a) which might be primarily the result of the strong increase in R_{Pol} of 30% (see Fig. 4b). This strong increase of R_{Pol} might be attributed to high diffusion losses due to non-desorbed tar species or benzene. As R_{Pol} significantly decreased after 10 h of operation with reference gas, these diffusion losses might have been the result of non-desorbed tar compounds rather

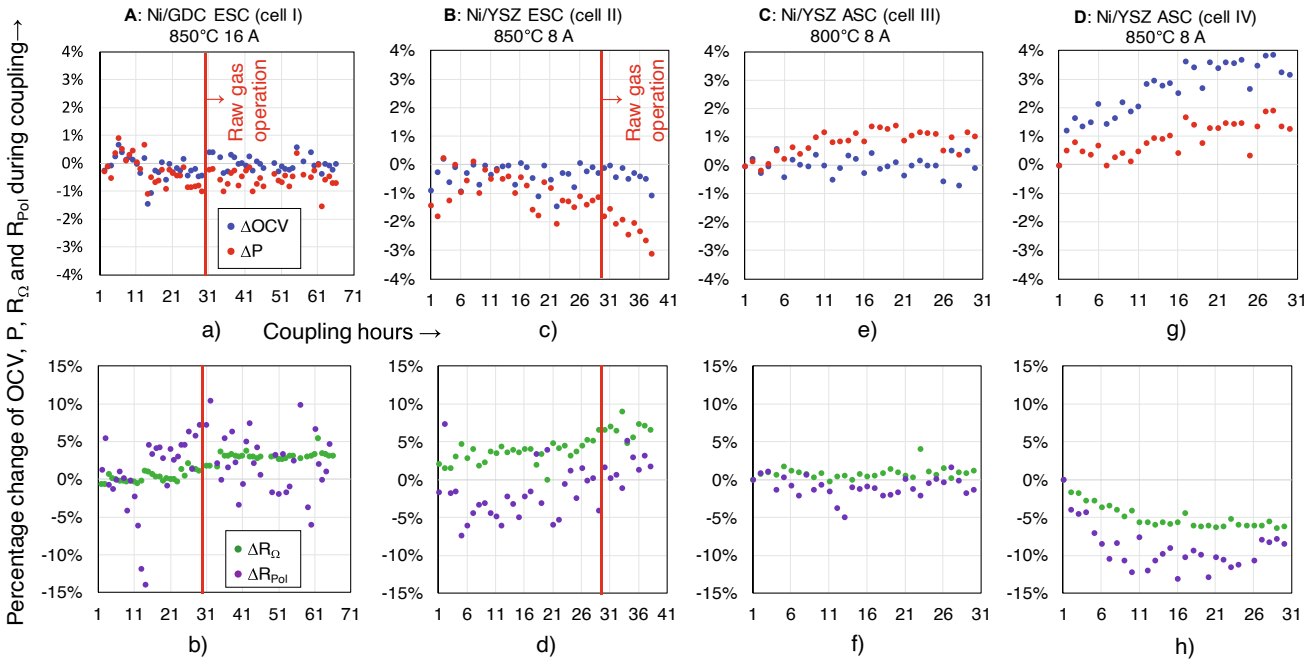

Fig. 3. Evolution of changes in cell performance (ΔP), open circuit voltage (ΔOCV), ohmic resistance (ΔR_Ω) and polarization resistance (ΔR_{Pol}) during coupling operation. Abscissa shows the operating hours on gasifier product gas. Reference gas operation between conditioned- and raw gas operation in tests A and B according to Fig. 2 are not displayed.

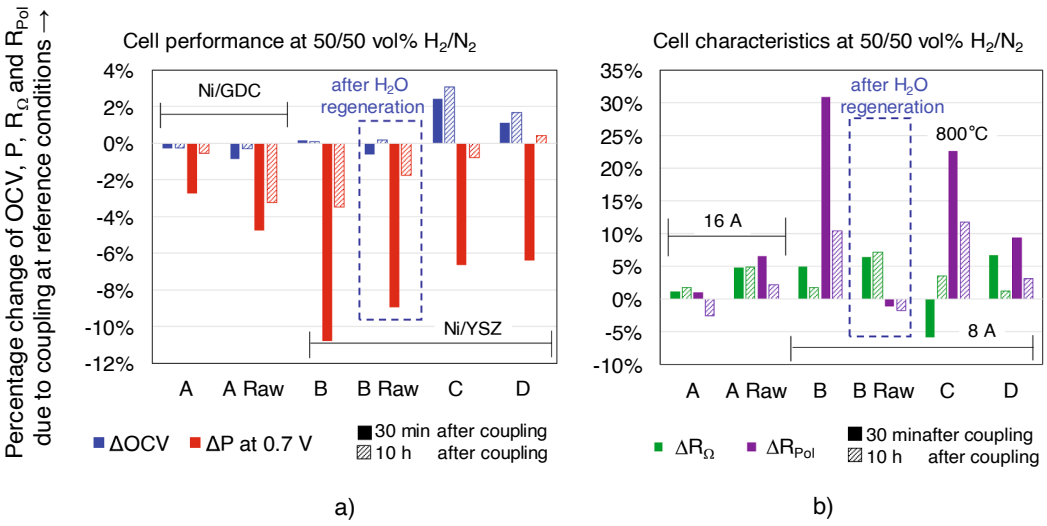

Fig. 4. Changes of a) cell power output at 0.7 V and OCV as well as b) cell resistances measured at 16 A (test A) and 8 A (tests B-D) due to coupling operation. Values determined 30 min (filled bars) and 10 h (hatched bars) after end of coupling in reference gas mixture of 50/50 vol% H_2/N_2. Between measurements, the cell was operated with 10/90 vol% H_2/N_2 at open circuit. Results for test B Raw after 10 h regeneration with 50/50 vol% H_2/H_2O mixture.

than carbon deposits. An irreversible performance loss of 3% after operation with conditioned product gas could be however observed, which is comparable to the irreversible loss at test A (Ni/GDC) using raw product gas, confirming the higher sensitivity to tars of Ni/YSZ in comparison to Ni/GDC.

After switching to raw product gas, a significantly faster performance decrease as a result of an increase in cell resistances could be observed as shown in Fig. 3c and d. Due to a failure in the fuel supply line of the gasifier after 10 h of raw gas operation and the already high performance degradation, it was decided to investigate if this performance degradation is recoverable. Therefore, a regeneration gas composition of 50/50 vol% H_2/H_2O was applied for 10 h. After this recovery phase, a cell performance decrease of 9% could be observed which however decreased down to 2% after 10 h of operation with 10 vol% H_2 in N_2 (see Fig. 4a). Considering the low polarization resistance in Fig. 4b, it can be assumed that possible carbon deposits were removed during the regeneration phase, whereby the large irreversible increase in ohmic resistance (approx. 7%) indicates damages to the uppermost anode layer, which is important for electrical contact. Post-mortem analyses confirmed these assumptions: No carbon deposition could be found on the cell anode whereby delamination of the upper most anode layer occurred in the center area of the flow field (details see section 3.3.2).

3.1.3. Test C - Ni/YSZ ASC 800°C

Ni/YSZ ASCs are widely used in industrial applications, especially when operating temperatures below 800°C are targeted. Therefore, the operation of this cell type with FBS product gas was focused in tests C and D using cell III and IV, respectively. The results from test B indicated that heavy tars (as present in raw product gas) might lead to severe damages of Ni/YSZ-based anodes. Therefore, operation with raw gas was avoided further on. Moreover, stable cell operation with gasifier product gas containing tar levels exceeding 1 mg·Nm^{-3} could not be demonstrated in the past for this cell type, even when SCRs were high (details see Table 2). To estimate the risk for carbon deposits at 700°C for the setup used in this work, 1 slpm of raw product gas was led through the alumina housing containing nickel meshes but no SOFC for 10 h in an additional experiment. The formation of a severe quantity of carbon could be observed (details see supplementary material Fig. S4), for which reason test C was conducted at 800°C.

In test C, the cell did not show any signs of performance degradation or increase in cell resistances (see Fig. 3 e, f) after 30 h of coupling. A performance increase of approx. 1% during 30 h of operation could even be observed, which might be attributed to a slightly increasing methane reforming capability (initial: 30%, after 30 h: 43%, details see supplementary material Fig. S2e). Simultaneously, a decrease in tar reforming capability was observed (details see section 3.2). Whereas no increase in OCV could be observed during operation, Fig. 4a shows a significant increase in OCV at reference conditions which could be attributed to a slight reduction of air leakages due to coupling operation according to GA analyses at reference conditions. Nevertheless, this increase in OCV might have compensated the irreversible increase of R_Ω and R_{Pol} shown in Fig. 4b, thus resulting in an irreversible performance degradation below 1%. The 5% lower R_Ω directly after test C might be attributed to beginning carbon formation in the uppermost anode layer thus increasing its conductivity according to [50]. For tests A, B and D conducted at 850°C, carbon deposition on the anode was thermodynamically less likely according to [49], which might explain why no decrease in R_Ω directly after coupling could be observed. According to post-test analyses presented in section 3.3.3, the largest amount of carbon deposits could be observed on the alumina cell holder and nickel meshes after test C, which might support the assumption that a thin carbon layer was formed on the anode during coupling. The additional steam produced during the recording of the current–voltage curve at reference conditions (50/50 vol% H_2/N_2) might have supported carbon reforming according to Eq. (7) and consequently the removal of these deposits. This carbon removal might have resulted in gaps between the anode layer and the contact meshes (foremost occupied by carbon) thus resulting in a worse electrical contact, which might explain the approx. 4% irreversible increase of R_Ω.

3.1.4. Test D - Ni/YSZ ASC 850°C

In test D, another Ni/YSZ ASC (cell IV) with thinner anode than the ASC from test C (cell III) was used and the temperature increased to 850°C in order to increase the comparability of degradation and carbon deposition with test A due to a comparable tar decomposition activity at 850°C, however considering a different anode material (test A: Ni/GDC; test D: Ni/YSZ). A steady performance and OCV increase up to 4% and 2%, respectively, could be observed at the beginning of the coupling operation with conditioned gas (see Fig. 3g) stabilizing after approximately 17 h. The gas analysis showed an increasing methane reforming capability during coupling (initial: 24%, after 15 h: 54%, after 30 h: 61%, details see supplementary material Fig. S2e). Thus, the methane reforming capability of both applied Ni/YSZ ASCs improved during the operation with tar-laden product gas from biomass gasification.

Simultaneously, as also observed in test C, a decrease in tar reforming capability was observed (details see section 3.2). This might depict, that methane reforming reactions occur preferentially on Ni/YSZ-based anodes compared to tar reforming reactions. Taking also the results from test C into consideration, a higher operating temperature might encourage this effect, possibly due to the faster kinetics and a faster desorption of light tar compounds occupying active nickel centers and hindering reforming reactions as discussed for naphthalene in [14]. As already observed for the Ni/YSZ ASC in test C, an increase in OCV under reference conditions is demonstrated in Fig. 4a whereas almost no difference in cell performance could be observed 10 h after coupling. However, Fig. 4b shows a much lower R_{Pol} in comparison to test C which might depict, that already more tar species desorbed in the 30 min between the end of the coupling and the first reference measurement due to the 50 K higher operating temperature. The higher methane reforming capability resulted in larger H_2 and CO quantities and a temperature decrease, which increased the OCV and consequently the power output. Besides, the larger H_2 concentration in the cell might explain the decreasing R_{Pol} according to the results presented in [27]. In contrast, an increase in R_Ω was expected due to the falling cell temperature, whereby the opposite could be observed as depicted in Fig. 3h. The formation of a thin carbon layer on the Ni/YSZ anode thus increasing the electrical contact and lowering R_Ω (as assumed for cell III in test C considering [50]), however, seems implausible when considering the higher R_Ω at reference conditions 30 min after coupling. Nevertheless, small steam contents in the reference gas as a result of minor air leakages combined with faster reforming kinetics at the elevated temperature might have promoted the removal of this possible thin carbon layer, which could have resulted in an increased R_Ω directly after coupling according to Fig. 3h as observed in tests A and B at 850°C. Additional experiments with real product gas focusing on the increasing methane steam reforming capability of cells with Ni/YSZ-based anode and the possible formation of a thin carbon layer enhancing electrical conductivity are recommended for the future.

In summary, a good performance stability of the cell with Ni/GDC-based anode (cell I) could be demonstrated when operated with tar-laden product gas at 850°C, which was also claimed previously by Hofmann et al. In contrast to [33] and [32], however, a product gas with a much lower SCR was used and fuel utilization was significantly reduced to encourage degradation as a result of carbon deposition in the cermet according to [49]. Nevertheless, a stable operation at 850°C with conditioned and raw product gas containing 3.7 and 4.8 g·Nm^{-3} d.b. gravimetric tars, respectively, for 30 h each was demonstrated. However, an irreversible performance degradation of 3% at reference conditions could be observed after raw gas operation, which can be attributed to the heavy tars which were not removed in the condenser for this case. Therefore, it can be assumed that cells with Ni/GDC-based anodes show a high potential for stable long-term operation when using real gasifier product gas with a reduced content of heavy tars and an industrial-relevant SCR.

A stable operation of Ni/YSZ ASCs for 30 h at 800°C and 850°C (cell III and IV) using a conditioned product gas with 3.2–3.4 g·Nm^{-3} d.b. gravimetric tar content was demonstrated. In addition, an increasing methane reforming capability was observed during coupling operation, which was more pronounced at 850°C than at 800°C. This increase in methane reforming capability, however, simultaneously resulted in a lower tar conversion (details see section 3.2). In contrast, a slight performance reduction could be observed for the Ni/YSZ ESC (cell II) when operated with conditioned product gas even at 850°C. The operation with raw product gas lead to severe performance degradation, which could be only partially recovered by applying a 50/50 vol% H_2O/H_2 gas mixture for 10 h. For this reason, the use of an ASC design for cells with Ni/YSZ-based anode might be recommended when tars are present in the product gas. In all tests, a performance reduction could be measured at reference conditions directly after coupling, which however decreased after 10 h under standby conditions (see Fig. 4). The same behavior could be observed for the polarization resistances in Fig. 3, which indicates that the desorption of steam, light tar compounds and benzene might take several hours. A higher desorption rate might be however claimed for cells with Ni/GDC-based anode in comparison to cells with Ni/YSZ-based anode.

In the past, a successful operation of Ni/YSZ ASCs with real product gas from biomass gasification could only be demonstrated in cases where the SCR was significantly higher than presented in this study [16] and the tar level was negligibly low [28], often combined with a high fuel utilization [16,28]. This study demonstrates that a stable operation of cells with Ni/YSZ-based anodes on gasifier product gas with industrial-relevant SCR at 800°C might be feasible for industrial applications if the content of heavy tars is reduced upstream of the cell.

3.2. Tar analysis

Tars were collected before and after the cell via the tar protocol to investigate the tar conversion capability of the cell and setup in each test. Table 6 shows the conversion of gravimetric tars as well as toluene and benzene during the coupling experiments. GC–MS analyses were conducted to determine the content of toluene representing light condensable class 3 tar compounds as well as benzene, which are not among the gravimetric tars due to their low boiling point. High conversion rates were achieved for the heavier gravimetric tars and also for light condensable tars and benzene in all experiments.

The decomposition of tars at SOFC operating conditions might be predominantly attributed to reforming reactions with steam (Eq. (3)) and/or carbon dioxide (Eq. (4)) and also thermal decomposition (Eq. (5)) according to [51]. These reactions are strongly endothermic resulting in favored forward reactions at elevated temperatures, whereby nickel (as present in SOFC anodes) acts as a catalyst according to [13]. Thus, a larger catalytically active surface as present in ASC SOFCs might indicate a higher tar conversion rate. However, an unexpected lower tar conversion rate could be observed in tests C and D using Ni/YSZ ASCs according to Table 6. In these tests, the increasing methane reforming capability throughout the 30 h of coupling with conditioned product gas (details see supplementary material Fig. S2 d and e) might depict that kinetics of catalytic methane steam reforming are faster than of catalytic tar reforming. This might explain the increase in methane reforming capability with a simultaneous decrease in tar conversion capability.

Carbon deposits might result from thermal decomposition of tars (Eq. (5)), the Boudouard reaction (Eq. (6)) and/or reversible carbon reforming (Eq. (7)). However, when considering the exothermic nature of the Boudouard and reversible carbon reforming reaction, carbon deposition might predominantly occur as a result of the thermal decomposition of tars at high temperatures. Von Berg et al. presented a significant reduction of gravimetric tars when increasing the temperature of a steam gasifier reactor from 700°C to 800°C [38], which might

Table 6
Conversion of gravimetric tars, toluene (representing the predominant light condensable class 3 tar) and benzene during coupling experiments.

[g·Nm^{-3} d.b.]	A	A Raw	B	B Raw	C	D
Temperatures	850°C	850°C	850°C	850°C	800°C	850°C
			Gravimetric tars			
Before cell	3.66	4.75	2.76	4.57	3.22	3.44
After cell	0.17	0.03	0.14	0.12	0.29	0.43
Conversion	95.4%	99.4%	94.9%	97.4%	91.0%	87.5%
			Benzene			
Before cell	7.25	8.26	8.49	8.58	8.29	7.58
After cell	0.10	0.02	0.26	0.00	0.41	0.64
Conversion	98.6%	99.7%	96.9%	100.0%	95.1%	91.5%
			Toluene			
Before cell	1.79	0.91	1.23	0.90	1.28	1.01
After cell	0.02	0.01	0.00	0.00	0.03	0.03
Conversion	99.0%	99.1%	100.0%	100.0%	97.6%	97.4%

indicate that the thermal decomposition of gravimetric tars and consequently the formation of solid carbon (see Eq. (5)) is possible in the absence of a nickel catalyst and therefore on the alumina support of the fuel cells at 800 and 850°C considered in this work. Moreover, nickel acts as a catalyst for reforming reactions thus reducing the risk for carbon deposition on the anode and meshes. Therefore, it is most likely that carbon deposits might be expected on the alumina support rather than the nickel meshes and the anode. This could be observed in post-mortem analyses presented in section 3.3.

$$C_xH_y + xH_2O \rightarrow xCO + (x + y/2)H_2 \quad (3)$$

(steam reforming, endothermic)

$$C_xH_y + xCO_2 \rightarrow 2xCO + y/2H_2 \quad (4)$$

(dry reforming, endothermic)

$$C_xH_y \leftrightarrow xC + y/2H_2 \quad (5)$$

(thermal decomposition, endothermic)

$$2CO \leftrightarrow C + CO_2 \quad (6)$$

(Boudouard reaction, exothermic)

$$CO + H_2 \leftrightarrow C + H_2O \quad (7)$$

(reversible carbon reforming, exothermic)

3.3. Post-mortem analyses

The cell assembly was investigated after each experiment for macroscopic carbon deposits and structural changes of the anode. Thermodynamic equilibrium calculations based on the Gibbs energy minimization method were conducted in advance to determine the thermodynamic boundaries for carbon deposition. According to these calculations, carbon deposits should not be likely on alumina parts, nickel meshes and the anode (details see supplementary material Fig S3). However, no kinetic effects were considered in this approach. In the previous section, it was assumed that carbon deposition might be expected at the investigated operating temperatures as a result of the thermal decomposition of tars. Post-test analyses of the setup proved this assumption, since macroscopic carbon deposits could be found on the alumina support after each experiment as shown in Fig. 5. However, the quantity of carbon and also its structure varied between each test, which is discussed below.

3.3.1. Test A - Ni/GDC ESC 850°C

In test A, carbon was deposited on the alumina parts in a very thin layer especially in the flow distributor and in the first half of the flow field (see Fig. 5a top). The silvery luster of the carbon deposits as well as their stability against mechanical abrasion indicated a graphitic nature. No macroscopic signs for carbon deposits could be found on the nickel mesh and anode. SEM analyses showed neither structural changes of the anode nor microscopic carbon deposits. Moreover, EDX analyses showed no increase of the carbon peak comparing points one and two of Fig. 5 a for anode and mesh (details see supplementary material Fig. S5). However, structural changes could be observed in parts of the nickel mesh reaching into the flow distributor. Fig. 6a shows a beginning separation of single nickel grains from the wires, a possible precursor for nickel dusting. Moreover, tree-shaped structures growing from the nickel wires could be identified as pyrolytic carbon via EDX. In the first centimeter of the flow field, no structural changes of the nickel wires could be observed, as shown in Fig. 6b. However, pyrolytic carbon tree structures could be identified to a lower extent as well as spherical nickel deposits, possibly released from the region shown in Fig. 6a. No such carbon structures and nickel deposits could be observed on the mesh in the center and outlet area. To sum up, SOFCs with Ni/GDC-based anodes can be claimed as robust against structural degradation and carbon deposits when operated with raw gasifier product gas containing significant amounts of heavy tars. This was also claimed in [32] for experiments with a maximum duration of 7 h and a significantly higher SCR of 7. However, the beginning of nickel dusting at the mesh might be a precursor for possible dusting effects at the anode during long-term operation.

3.3.2. Test B - Ni/YSZ ESC 850°C

In test B, 30 h of operation with conditioned product gas and 12 h with raw gas were followed by a 10 h regeneration period with 50/50 vol% H_2/H_2O regeneration gas (see Fig. 3c). Due to the high steam content of the regeneration gas, less carbon deposits were expected taking the steam reforming of carbon into consideration (see Eq. (7)). Fig. 5b shows significantly less carbon deposits on the alumina parts of

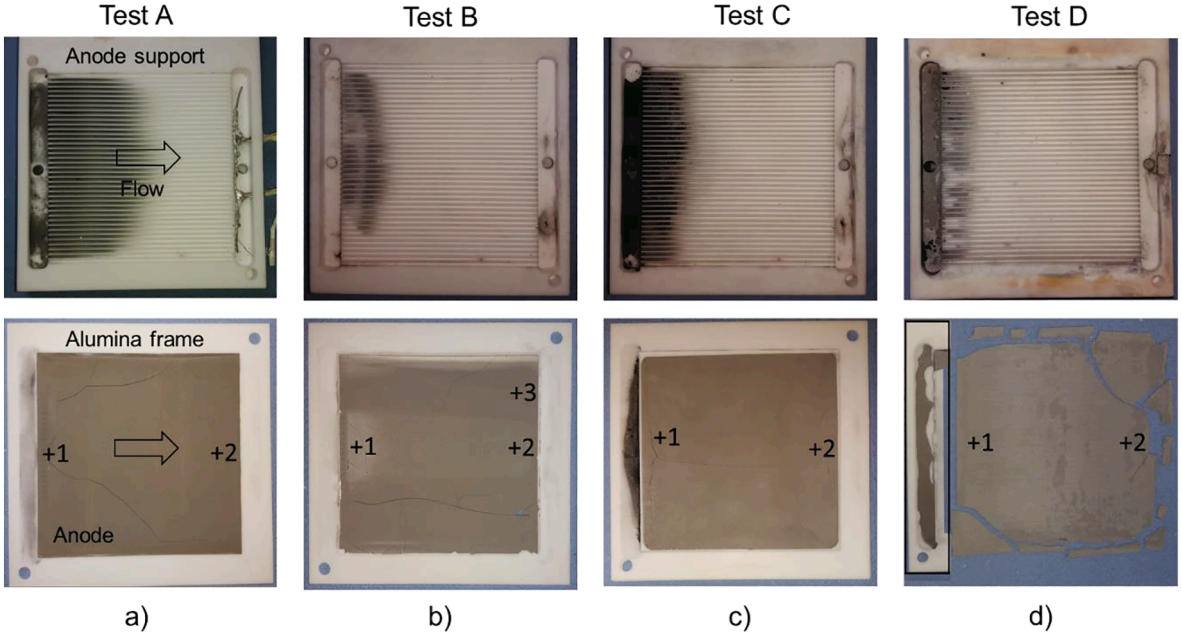

Fig. 5. Alumina cell holder (top) and cell anode (bottom) showing carbon deposits on alumina and structural changes of cell anodes I-IV for tests A – D.

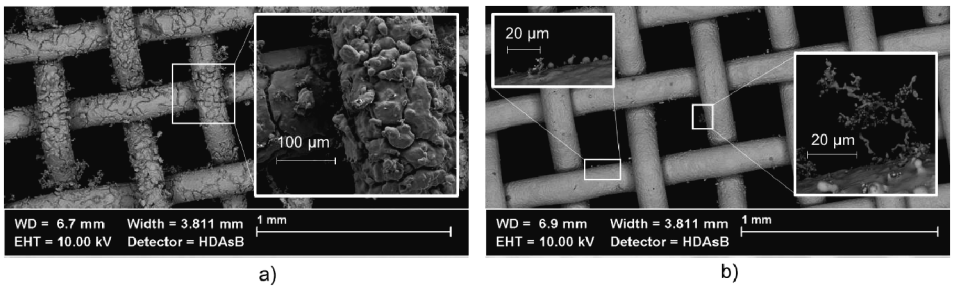

Fig. 6. SEM analysis of Test A: a) Start of nickel dusting for the nickel mesh reaching into the flow distributor before reaching the cell. b) Nickel mesh at the beginning of the flow field showing not structural changes but spherical nickel deposits and pyrolytic carbon structures.

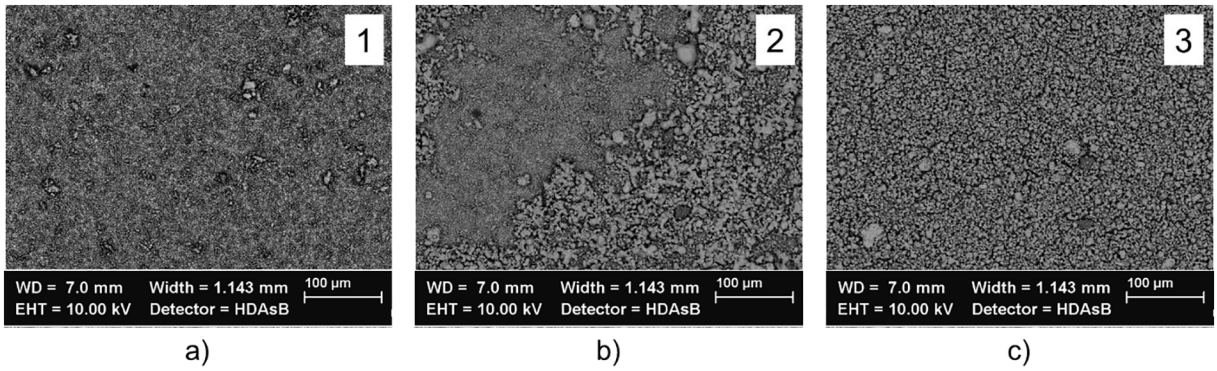

Fig. 7. SEM analysis of Test B: Ni/YSZ ESC anode (cell II) in the middle of the flow field at a) inlet and b) outlet according to Fig. 5b with strong anode delamination in comparison to c) intact anode.

test B in comparison to test A. Especially in the flow distributor, an area with low gas velocity, full carbon removal could be observed. No carbon deposits could be found on the anode or nickel mesh during SEM analyses. EDX analysis also showed no increase of the carbon peak comparing point one and two of Fig. 5b for anode and mesh (details see supplementary material Fig. S5). Similar to test A, nickel dusting occurred on parts of the nickel mesh reaching into the flow distributor. Moreover, strong delamination of the anode could be observed in the center area of the flow field. Delamination however decreased in flow direction (see Fig. 5b bottom and Fig. 7a/b). The border areas of the flow field showed no anode delamination or other structural changes of the anode (see Fig. 7c). Comparable delamination effects were observed in the past on Ni/YSZ ASCs operated at 700°C with simulated gasifier product gas containing up to 8 g·Nm^{-3} phenol [52] and at 715°C using real product gas containing up to 5 g·Nm^{-3} tars [15]. Heavy tars like phenol were also present in the raw product gas of the experiments presented in this study. It thus can be assumed, that structural degradation of Ni/YSZ-based anodes cannot be avoided when cells are operated with raw product gas containing approximately 5 g·Nm^{-3} gravimetric tars, even at 850°C.

3.3.3. *Test C - Ni/YSZ ASC 800°C*

Carbon deposits on the alumina cell assembly of test C differed significantly in their characteristics from the deposits of tests A and B. The density of the carbon deposits appeared to be significantly lower than those of the graphitic deposits of test A and B thus showing a higher tendency to block the flow channels in the further course of the operation. Moreover, the black coloring and instability against mechanical abrasion of the deposits led to the assumption that carbon deposits from test C were of pyrolytic nature according to [53]. In contrast to test A and B, carbon deposits could also be found in the alumina fuel gas supply line. Therefore, the 50 K lower temperature of test C compared to the other tests could have had a significant effect on the amount and structure of carbon deposits. An additional experiment at further lowered temperature of 700°C using the presented setup with an alumina cover containing a nickel mesh but no SOFC demonstrated severe formation of pyrolytic carbon already after 10 h of operation with 1 slpm raw product gas (details see supplementary material Fig. S4). In contrast to the carbon deposits of test A-D, pyrolytic carbon structures started to grow from the nickel mesh towards the alumina support which might be attributed to a shift of the equilibrium of the exothermic reversible carbon reforming reaction (Eq. (7)) and Boudouard reaction (Eq. (6)) towards carbon formation. In summary, this result demonstrates the increasing risk for the formation of pyrolytic carbon deposits in quantities which will have severe effects on the SOFC operation even at a product gas SCR of approximately 2 at temperatures below 800°C.

The Ni/YSZ anode of the ASC used in test C (cell III) did not show any macroscopic signs of structural degradation of the anode. SEM analyses of the anode in the inlet and outlet area numbered as 1 and 2 in Fig. 5c, respectively, did not indicate any carbon deposits. However, an increase of the oxygen and zirconia peak could be observed in EDX spectra (details see supplementary material Fig. S5). This might indicate an enrichment of zirconia in the cermet as a possible result of nickel dusting, which could not be confirmed, however, by SEM analysis. SEM analysis of the nickel mesh showed a different picture. Pyrolytic tree-shaped carbon structures comparable to the ones discussed for test A as well as flat carbon deposits could be observed on the mesh closest to the alumina flow field as shown in Fig. 8a. The nickel mesh below did not show any signs of carbon deposits. Therefore, it might be assumed that carbon deposits are formed starting from the alumina support rather than from the catalytically active anode. This would also correlate with the observation that no carbon could be found on the anode whereas deposits were visible on the alumina support.

3.3.4. *Test D - Ni/YSZ ASC 850°C*

In test D, a Ni/YSZ ASC (cell IV) was operated at 850°C with conditioned product gas for 30 h. Carbon deposits again appeared to be of graphitic nature, which was already observed in test A and B. In

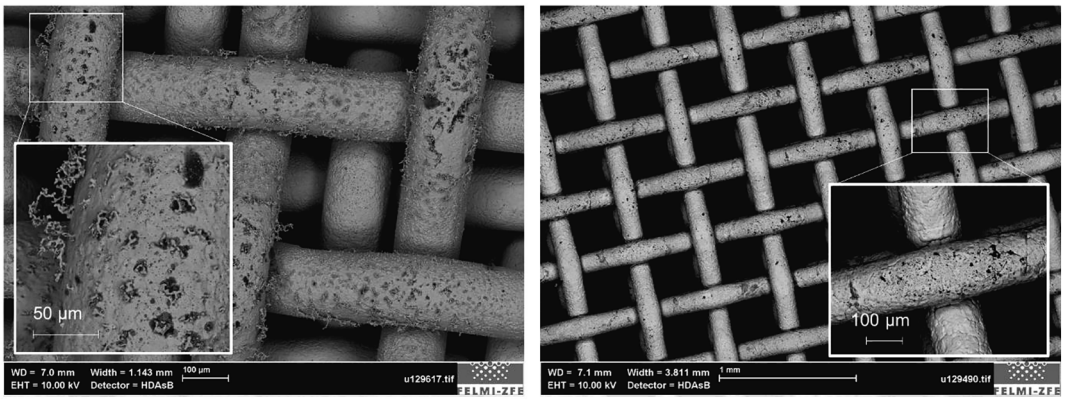

Fig. 8. SEM analysis of nickel mesh compound from a) the inlet area of test C and b) from the outlet area of test D showing carbon structures and flat carbon deposits, respectively. Upper mesh layer in contact with alumina flow field.

contrast to test A, carbon predominantly deposited in the flow distributor rather than the flow channels (see Fig. 5d top). This might be attributed to the lower carbon quantity passing through the cell holder due to raw gas operation avoidance and a slightly lower volume flow rate according to Table 5. Similar to tests A and C, no macroscopic delamination effects or carbon deposits could be observed on the anode or nickel mesh. This circumstance might prove that the anode delamination observed in test B can be attributed to tar compounds from the raw gas. However, SEM analyses revealed carbon deposits on the nickel mesh in the outlet region of the cell as shown in Fig. 8b. The quantity of carbon deposits increased in the flow direction according to EDX analyses. A slight increase of the carbon content detected by EDX was also observed for the anode (details see supplementary material Fig. S5). However, no carbon deposits were visible on the cermet in the SEM analyses.

In summary, carbon deposits could be avoided on Ni/GDC and Ni/YSZ anode cermets at 800°C and 850°C operating temperatures. This might be attributed to thermal decomposition of tar compounds primarily in the alumina support and on the nickel meshes rather than on the anode. Moreover, an increasing risk of pyrolytic carbon formation with decreasing temperature was demonstrated. In contrast to graphitic carbon formed at 850°C, pyrolytic carbon already forms at 800°C during the operation with conditioned product gas and might lead to blockages in the flow field in a significantly shorter period of time due to its lower density. Considering the risk for carbon deposition, it might therefore be advisable to either aim for operating temperatures exceeding 800°C when operating SOFCs with tar-laden product gases from biomass gasification or to increase the SCR of the product gas as investigated in [16] and [32].

Concluding, carbon deposition in the flow distributor and the flow channels might be the limiting factor causing an early shut-down of SOFC stacks rather than carbon hindering diffusion within the cermets. The operation of cells on raw product gas led to nickel dusting of the mesh within the first millimeters of the flow field for both experiments. Whereas heavy tars did not lead to dusting effects in the Ni/GDC cermet of cell I, severe dusting could be observed for the Ni/YSZ cermet of cell II. This correlates with the existing literature summarized in [17], in which a higher stability against structural degradation and carbon deposition is claimed for cells with Ni/GDC-based anodes in comparison to cells with Ni/YSZ-based anodes. SOFC operation on raw product gas containing heavy tars might therefore lead to accelerated degradation of SOFCs. However, the reduction of heavy tars might already be sufficient to ensure stable operation, especially at SOFC operating temperatures exceeding 800°C. Whereas cells with Ni/GDC-based anodes are already known for their higher stability against structural degradation, a degradation-free operation of cells with Ni/YSZ-based anodes with tar laden product gas and a SCR of approx. 2 for at least 30 h could be demonstrated for the first time.

4. Conclusions and outlook

Fluidized bed steam gasifiers offer the potential to increase the efficiency of biomass gasification-based CHPs using SOFCs as power generators due to their high fuel flexibility and a product gas composition very suited for the utilization in SOFCs. However, the significantly higher tar content in comparison to air gasifiers may demand a more intensive gas cleaning and higher SCR of the product gas for the operation with SOFCs, which would increase costs and decrease the cell performance. For this reason, results from successfully operating SOFCs with real product gas from steam gasification showing moderate SCRs and the presence of tars are of high value due to a potential in reducing gas cleaning costs besides increasing the expectable cell performance.

For the first time, SOFC operation with real product gas from steam gasification containing a typical amount of tars for fluidized bed gasification (2.8 to 4.8 $g \cdot Nm^{-3}$ d.b.) at an industrial-relevant steam-to-carbon ratio (approx. 2) could be demonstrated for dozens of hours showing following results:

- A stable operation without structural degradation over 60 h could be demonstrated for a Ni/GDC ESC at 850°C whereby raw product gas was used for 30 h. Although raw gas operation did not lead to structural degradation of the anode, metal dusting of the nickel mesh and an irreversible 3% performance degradation at reference conditions (H_2/N_2 mixture) could be observed. Thus, the used cell type demonstrated a high potential for future long-term operation, which was also assumed in previous studies. However, heavy tars should be avoided to decrease the risk for dusting effects at the contacting meshes, as no irreversible performance degradation was present when a conditioned gas (with removal of heavy tars) was employed.
- In contrast, severe metal dusting of the anode and nickel meshes and consequently an irreversible performance loss could be demonstrated for a Ni/YSZ ESC after 30 h and 12 h of operation with conditioned (less tar content after removing heavier tars) and raw product gas at 850°C, respectively. Thus, Ni/YSZ-based anodes might not be suitable for the operation with gases containing heavy tars, even at comparably high temperatures.
- ASCs with Ni/YSZ-based anodes showed an increase of performance in time when operated with a conditioned gas where only the heavy tars are removed, both at 800 and 850°C and at moderate electrical load. For both cases, a 6% performance reduction was observed at reference conditions (H_2/N_2 mixture) directly after coupling operation which however recovered within 10 h without structural

degradation of the anodes. In contrast, a performance reduction could be observed for the Ni/YSZ ESC when operated with conditioned product gas even at 850°C. Thus, the operation of Ni/YSZ ASCs might be feasible if the content of heavy tars is reduced and operating temperatures are set to at least 800°C.

- In contrast to thermodynamic predictions, carbon deposition on the alumina support could be observed spreading towards the meshes, but not reaching the anodes. This might indicate that carbon deposits predominantly result from the thermal decomposition of tars. When increasing the temperature from 800°C to 850°C, a change from a pyrolytic to a graphitic structure of carbon deposits could be observed thus significantly reducing the risk for blockages in the flow channels. Therefore, temperatures exceeding 800°C might be advisable for SOFC operation with a tar-laden product gas to avoid carbon induced degradation.
- Carbon could be removed from the alumina support to a great extent by applying a H_2/H_2O regeneration gas mixture for 10 h at 850°C. This result might be considered for future regeneration strategies.
- High conversion rates of gravimetric tars, toluene and benzene during coupling operation could be observed. This demonstrates the low stability not only of gravimetric tars but also of light condensable tars and benzene in a SOFC cell assembly. The thermal decomposition of tars might have been the main source for carbon deposition.

In conclusion, the reduction of heavy tars, although modest in the percentage of reduction of the total tar content, proved to be extremely relevant to avoid changes in the morphology of both Ni/ceria- and Ni/zirconia-based anodes and consequently to avoid performance degradation. At 850°C, an SCR of 2 might be sufficient to avoid carbon deposits on cell anodes and to ensure a graphitic structure of deposits on the cell support thus reducing the risk of fast blockages in the flow channels. Moreover, tar-induced structural degradation of Ni/zirconia-based anodes might be avoided at this temperature and SCR despite their known lower tolerance to tars in comparison to Ni/ceria-based anodes. However, higher fuel cell operating temperatures (850°C) increase the risk for temperature-activated degradation phenomena which strongly affect the long-term durability of fuel cells. Moreover, higher temperatures increase the demands on the stack/system balance of plant, e.g. in terms of interconnect materials, sealing materials, recirculation devices and heat recovery. These points have to be considered for the selection of proper cell types and operating conditions for biomass-to-power systems using SOFCs as power generators. For the future, further experimental studies are suggested using metal-based cell assemblies in order to investigate, if the presented results can be reproduced for such industrial-relevant setups. Moreover, experiments with steam addition to the product gas might help to determine the necessary SCR in order to avoid carbon deposition at temperatures below 800°C, especially when considering higher industrial-relevant fuel utilization rates.

CRediT authorship contribution statement

Gernot Pongratz: Conceptualization, Methodology, Investigation, Validation, Data curation, Writing – original draft. **Vanja Subotić:** Funding acquisition, Methodology, Validation, Writing – review & editing, Supervision. **Lukas von Berg:** Investigation. **Hartmuth Schroettner:** Investigation. **Christoph Hochenauer:** Project administration, Resources. **Stefan Martini:** Conceptualization. **Maximilian Hauck:** Methodology, Investigation, Validation, Writing – review & editing. **Benjamin Steinruecken:** Methodology, Investigation, Validation, Writing – review & editing. **Marek Skrzypkiewicz:** Methodology, Validation, Writing – review & editing. **Jakub Kupecki:** Methodology, Validation, Writing – review & editing. **Robert Scharler:** Funding acquisition, Writing – review & editing, Supervision. **Andrés Anca-Couce:** Funding acquisition, Conceptualization, Methodology, Validation, Writing – review & editing, Supervision.

Declaration of Competing Interest

The authors declare that they have no known competing financial interests or personal relationships that could have appeared to influence the work reported in this paper.

Acknowledgements

The financial support by the Austrian Federal Ministry for Climate Action, Environment, Energy, Mobility, Innovation and Technology (BMK) [grant number 869036] and the Polish National Centre for Research and Development [grant number BIOENERGY-11/BIO-CCHP/2018] for the BIO-CCHP project within the framework of the 11th Joint Call of ERA-NET Bioenergy as well as the European Union's Horizon 2020 Research and Innovation Program [grant number 731101] for the BRISK II project is gratefully acknowledged. Moreover, the provision of an anode supported cell by Forschungszentrum Jülich is gratefully acknowledged.

Appendix A. Supplementary data

Supplementary data to this article can be found online at https://doi.org/10.1016/j.fuel.2022.123310.

References

[1] Intergovernmental panel on climate change (IPCC). Special Report: Global Warming of 1.5 °C 2020. https://www.ipcc.ch/sr15/ (accessed September 21, 2020).
[2] Heidenreich S, Foscolo PU. New concepts in biomass gasification. Prog Energy Combust Sci 2015;46:72–95. https://doi.org/10.1016/j.pecs.2014.06.002.
[3] Wu Z, Zhu P, Yao J, Zhang S, Ren J, Yang F, et al. Combined biomass gasification, SOFC, IC engine, and waste heat recovery system for power and heat generation: Energy, exergy, exergoeconomic, environmental (4E) evaluations. Appl Energy 2020;279:115794. https://doi.org/10.1016/j.apenergy.2020.115794.
[4] Anca-Couce A, Hochenauer C, Scharler R. Bioenergy technologies, uses, market and future trends with Austria as a case study. Renew Sustain Energy Rev 2021;135:110237. https://doi.org/10.1016/j.rser.2020.110237.
[5] Subotić V, Baldinelli A, Barelli L, Scharler R, Pongratz G, Hochenauer C, et al. Applicability of the SOFC technology for coupling with biomass-gasifier systems: Short- and long-term experimental study on SOFC performance and degradation behaviour. Appl Energy 2019;256:113904. https://doi.org/10.1016/j.apenergy.2019.113904.
[6] Aravind PV, de Jong W. Evaluation of high temperature gas cleaning options for biomass gasification product gas for Solid Oxide Fuel Cells. Prog Energy Combust Sci 2012;38(6):737–64. https://doi.org/10.1016/j.pecs.2012.03.006.
[7] Papurello D, Chiodo V, Maisano S, Lanzini A, Santarelli M. Catalytic stability of a Ni-Catalyst towards biogas reforming in the presence of deactivating trace compounds. Renew Energy 2018;127:481–94. https://doi.org/10.1016/j.renene.2018.05.006.
[8] Ud Din Z, Zainal ZA. The fate of SOFC anodes under biomass producer gas contaminants. Renew Sustain Energy Rev 2017;72:1050–66. https://doi.org/10.1016/j.rser.2016.10.012.
[9] Costa P, Pinto F, André RN, Marques P. Integration of Gasification and Solid Oxide Fuel Cells (SOFCs) for Combined Heat and Power (CHP). Processes 2021;9:254. https://doi.org/10.3390/pr9020254.
[10] Cavalli A, Kunze M, Aravind PV. Cross-influence of toluene as tar model compound and HCl on Solid Oxide Fuel Cell anodes in Integrated Biomass Gasifier SOFC Systems. Appl Energy 2018;231:1–11. https://doi.org/10.1016/j.apenergy.2018.09.060.
[11] Papurello D, Silvestri S, Modena S. Biogas trace compounds impact on high-temperature fuel cells short stack performance. Int J Hydrog Energy 2021;46(12):8792–801. https://doi.org/10.1016/j.ijhydene.2020.11.273.
[12] Li Y, Pang Y, Tu H, Torrigino F, Biollaz SMA, Li Z, et al. Impact of syngas from biomass gasification on solid oxide fuel cells: A review study for the energy transition. Energy Convers Manag 2021;250:114894. https://doi.org/10.1016/j.enconman.2021.114894.
[13] Coll R, Salvadó J, Farriol X, Montané D. Steam reforming model compounds of biomass gasification tars: conversion at different operating conditions and tendency towards coke formation. Fuel Process Technol 2001;74(1):19–31. https://doi.org/10.1016/S0378-3820(01)00214-4.
[14] Hauth M, Lerch W, König K, Karl J. Impact of naphthalene on the performance of SOFCs during operation with synthetic wood gas. J Power Sources 2011;196(17):7144–51. https://doi.org/10.1016/j.jpowsour.2010.09.007.
[15] Jeong H, Hauser M, Fischer F, Hauck M, Lobe S, Peters R, et al. Utilization of Bio-Syngas in Solid Oxide Fuel Cell Stacks: Effect of Hydrocarbon Reforming. J Electrochem Soc 2019;166(2):F137–43. https://doi.org/10.1149/2.1191902jes.

[16] Fischer F, Hauser M, Hauck M, Herrmann S, Fendt S, Jeong H, et al. Effect of internal hydrocarbon reforming during coupled operation of a biomass gasifier with hot gas cleaning and SOFC stacks. Energy Sci Eng 2019. https://doi.org/10.1002/ese3.334.

[17] Liu M, Aravind PV. The fate of tars under solid oxide fuel cell conditions: A review. Appl Therm Eng 2014;70(1):687–93. https://doi.org/10.1016/j.applthermaleng.2014.05.068.

[18] Kaltschmitt M, Hartmann H, Hofbauer H, editors.. Energie aus Biomasse: Grundlagen, Techniken und Verfahren. 3, aktualisierte und. erweiterte Auflage. Berlin Heidelberg: Springer Vieweg; 2016.

[19] Bridgwater AV. The technical and economic feasibility of biomass gasification for power generation. Fuel 1995;74(5):631–53. https://doi.org/10.1016/0016-2361(95)00001-L.

[20] Zachl A, Buchmayr M, Gruber J, Anca-Couce A, Scharler R, Hochenauer C. Shifting of the flame front in a small-scale commercial downdraft gasifier by water injection and exhaust gas recirculation. Fuel 2021;303:121297. https://doi.org/10.1016/j.fuel.2021.121297.

[21] Forzatti P, Lietti L. Catalyst deactivation. Catal Today 1999;52:165–81. https://doi.org/10.1016/S0920-5861(99)00074-7.

[22] Lee WY, Hanna J, Ghoniem AF. On the Predictions of Carbon Deposition on the Nickel Anode of a SOFC and Its Impact on Open-Circuit Conditions. J Electrochem Soc 2013;160(2):F94–105. https://doi.org/10.1149/2.051302jes.

[23] Sasaki K, Teraoka Y. Equilibria in Fuel Cell Gases II. The C-H-O Ternary Diagrams. J Electrochem Soc 2003;150:A885–8. https://doi.org/10.1149/1.1577338.

[24] Schluckner C, Subotić V, Lawlor V, Hochenauer C. Carbon Deposition Simulation in Porous SOFC Anodes: A Detailed Numerical Analysis of Major Carbon Precursors. J Fuel Cell Sci Technol 2015;12:051007-051007–12. https://doi.org/10.1115/1.4031862.

[25] Subotić V, Schluckner C, Stöckl B, Lawlor V, Schroettner H, Hochenauer C. Strategy for Carbon Gasification from Porous Ni-YSZ Anodes of Industrial-Sized ASC-SOFCs and Effects of Carbon Growth. J Electrochem Soc 2016;163(14):F1515–22. https://doi.org/10.1149/2.0521614jes.

[26] Pashchenko D, Makarov I. Carbon deposition in steam methane reforming over a Ni-based catalyst: Experimental and thermodynamic analysis. Energy 2021;222:119993. https://doi.org/10.1016/j.energy.2021.119993.

[27] Pongratz G, Subotić V, Schroettner H, Stoeckl B, Hochenauer C, Anca-Couce A, et al. Investigation of solid oxide fuel cell operation with synthetic biomass gasification product gases as a basis for enhancing its performance. Biomass Convers Biorefinery 2021;11(1):121–39. https://doi.org/10.1007/s13399-020-00726-w.

[28] Gadsbøll RØ, Thomsen J, Bang-Møller C, Ahrenfeldt J, Henriksen UB. Solid oxide fuel cells powered by biomass gasification for high efficiency power generation. Energy 2017;131:198–206. https://doi.org/10.1016/j.energy.2017.05.044.

[29] Hofmann P, Schweiger A, Fryda L, Panopoulos KD, Hohenwarter U, Bentzen JD, et al. High temperature electrolyte supported Ni-GDC/YSZ/LSM SOFC operation on two-stage Viking gasifier product gas. J Power Sources 2007;173(1):357–66. https://doi.org/10.1016/j.jpowsour.2007.04.073.

[30] Motylinski K, Blesznowski M, Skrzypkiewicz M, Wierzbicki M, Zurawska A, Baran A, et al. Analysis of Soot Deposition Mechanisms on Nickel-Based Anodes of SOFCs in Single-Cell and Stack Environment. Processes 2020;8(11):1370. https://doi.org/10.3390/pr8111370.

[31] Karl J, Pröll T. Steam gasification of biomass in dual fluidized bed gasifiers: A review. Renew Sustain Energy Rev 2018;98:64–78. https://doi.org/10.1016/j.rser.2018.09.010.

[32] Hofmann P, Panopoulos KD, Aravind PV, Siedlecki M, Schweiger A, Karl J, et al. Operation of solid oxide fuel cell on biomass product gas with tar levels >10 g Nm−3. Int J Hydrog Energy 2009;34:9203–12. https://doi.org/10.1016/j.ijhydene.2009.07.040.

[33] HOFMANN P, PANOPOULOS K, FRYDA L, SCHWEIGER A, OUWELTJES J, KARL J. Integrating biomass gasification with solid oxide fuel cells: Effect of real product gas tars, fluctuations and particulates on Ni-GDC anode. Int J Hydrog Energy 2008;33(11):2834–44. https://doi.org/10.1016/j.ijhydene.2008.03.020.

[34] Pongratz G, Subotić V, Schroettner H, Hochenauer C, Skrzypkiewicz M, Kupecki J, et al. Analysis of H2S-related short-term degradation and regeneration of anode- and electrolyte supported solid oxide fuel cells fueled with biomass steam gasifier product gas. Energy 2021;218:119556. https://doi.org/10.1016/j.energy.2020.119556.

[35] Stoeckl B, Subotić V, Preininger M, Schroettner H, Hochenauer C. SOFC operation with carbon oxides: Experimental analysis of performance and degradation. Electrochim Acta 2018;275:256–64. https://doi.org/10.1016/j.electacta.2018.04.036.

[36] Tanaka T, Inui Y, Pongratz G, Subotić V, Hochenauer C. Numerical investigation on the performance and detection of an industrial-sized planar solid oxide fuel cell with fuel gas leakage. Appl Energy 2021;285:116426. https://doi.org/10.1016/j.apenergy.2020.116426.

[37] Soria-Verdugo A, Von Berg L, Serrano D, Hochenauer C, Scharler R, Anca-Couce A. Effect of bed material density on the performance of steam gasification of biomass in bubbling fluidized beds. Fuel 2019;257:116118. https://doi.org/10.1016/j.fuel.2019.116118.

[38] von Berg L, Pongratz G, Pilatov A, Almuina-Villar H, Hochenauer C, Scharler R, et al. Correlations between tar content and permanent gases as well as reactor temperature in a lab-scale fluidized bed biomass gasifier applying different feedstock and operating conditions. Fuel 2021;305:121531. https://doi.org/10.1016/j.fuel.2021.121531.

[39] Kienberger T, Zuber C, Novosel K, Baumhakl C, Karl J. Desulfurization and in situ tar reduction within catalytic methanation of biogenous synthesis gas. Fuel 2013;107:102–12. https://doi.org/10.1016/j.fuel.2013.01.061.

[40] Błesznowski M, Jewulski J, Zieleniak A. Determination of H2S and HCl concentration limits in the fuel for anode supported SOFC operation. Open Chem 2013;11:960–7. https://doi.org/10.2478/s11532-013-0228-1.

[41] Anca-Couce A, Brunner T, Kanzian W, Obernberger I, Trattner K. Characterization and condensation behaviour of gravimetric tars produced during spruce torrefaction. J Anal Appl Pyrolysis 2016;119:173–9. https://doi.org/10.1016/j.jaap.2016.02.020.

[42] Devi L, Ptasinski KJ, Janssen FJJG, van Paasen SVB, Bergman PCA, Kiel JHA. Catalytic decomposition of biomass tars: use of dolomite and untreated olivine. Renew Energy 2005;30(4):565–87. https://doi.org/10.1016/j.renene.2004.07.014.

[43] van de Kamp WL. de Wild PJ, Knoef HAM. Neeft JPA: Kiel JHA. Tar measurement in biomass gasification, standardisation and supporting R&D; 2006.

[44] Singhal SC, Kendall K, editors. High-temperature solid oxide fuel cells: fundamentals, design, and applicatons. New York: Elsevier Advanced Technology; 2003.

[45] KeraCell-III D, KERAFOL®,. Keramische Folien GmbH 2014.

[46] KeraCell-I D, KERAFOL®,. Keramische Folien GmbH 2014.

[47] Kupecki J, Kluczowski R, Papurello D, Lanzini A, Kawalec M, Krauz M, et al. Characterization of a circular 80 mm anode supported solid oxide fuel cell (AS-SOFC) with anode support produced using high-pressure injection molding (HPIM). Int J Hydrog Energy 2019;44(35):19405–11. https://doi.org/10.1016/j.ijhydene.2018.02.143.

[48] Schafbauer W, Menzler NH, Buchkremer HP. Tape Casting of Anode Supports for Solid Oxide Fuel Cells at Forschungszentrum Jülich. Int J Appl Ceram Technol 2014;11(1):125–35. https://doi.org/10.1111/ijac.2013.11.issue-110.1111/j.1744-7402.2012.02839.x.

[49] Singh D, Hernández-Pacheco E, Hutton PN, Patel N, Mann MD. Carbon deposition in an SOFC fueled by tar-laden biomass gas: a thermodynamic analysis. J Power Sources 2005;142(1-2):194–9. https://doi.org/10.1016/j.jpowsour.2004.10.024.

[50] Subotić V, Schluckner C, Strasser J, Lawlor V, Mathe Jörg, Rechberger Jürgen, et al. In-situ electrochemical characterization methods for industrial-sized planar solid oxide fuel cells Part I: Methodology, qualification and detection of carbon deposition. Electrochim Acta 2016;207:224–36. https://doi.org/10.1016/j.electacta.2016.05.025.

[51] Liu M, van der Kleij A, Verkooijen AHM, Aravind PV. An experimental study of the interaction between tar and SOFCs with Ni/GDC anodes. Appl Energy 2013;108:149–57. https://doi.org/10.1016/j.apenergy.2013.03.020.

[52] Jeong H, Geis M, Lenser C, Lobe S, Herrmann S, Fendt S, et al. Coupling SOFCs to biomass gasification – The influence of phenol on cell degradation in simulated bio-syngas. Part II – Post-test analysis. Int J Hydrog. Energy 2018;43(45):20911–20. https://doi.org/10.1016/j.ijhydene.2018.09.006.

[53] Sehested J. Four challenges for nickel steam-reforming catalysts. Catal Today 2006;111(1-2):103–10. https://doi.org/10.1016/j.cattod.2005.10.002.

[54] Pongratz G, Subotić V, Hochenauer C, Scharler R, Anca-Couce A. Solid oxide fuel cell operation with biomass gasification product gases: Performance- and carbon deposition risk evaluation via a CFD modelling approach. Energy 2022;244. https://doi.org/10.1016/j.energy.2021.123085.